



HAL
open science

The structural plasticity of the human copper chaperone for SOD1 - insights from combined size exclusion chromatographic and solution X-ray scattering studies

Gareth S. A. Wright, Syed Samar Hasnain, Jörg Günter Grossmann

► To cite this version:

Gareth S. A. Wright, Syed Samar Hasnain, Jörg Günter Grossmann. The structural plasticity of the human copper chaperone for SOD1 - insights from combined size exclusion chromatographic and solution X-ray scattering studies. *Biochemical Journal*, 2011, 439 (1), pp.39-44. 10.1042/BJ20110948 . hal-00628666

HAL Id: hal-00628666

<https://hal.science/hal-00628666>

Submitted on 4 Oct 2011

HAL is a multi-disciplinary open access archive for the deposit and dissemination of scientific research documents, whether they are published or not. The documents may come from teaching and research institutions in France or abroad, or from public or private research centers.

L'archive ouverte pluridisciplinaire **HAL**, est destinée au dépôt et à la diffusion de documents scientifiques de niveau recherche, publiés ou non, émanant des établissements d'enseignement et de recherche français ou étrangers, des laboratoires publics ou privés.

The Structural Plasticity of the Human Copper Chaperone for SOD1 - Insights from Combined Size Exclusion Chromatographic and Solution X-Ray Scattering Studies

Gareth S.A. Wright, S. Samar Hasnain and J. Günter Grossmann

Molecular Biophysics Group, Institute of Integrative Biology, Faculty of Health and Life Sciences,
University of Liverpool, Crown Street, Liverpool L69 7ZB

Abstract

The incorporation of copper into biological macromolecules such as Cu-Zn superoxide dismutase (SOD1) is essential for the viability of most organisms. However, copper is toxic and therefore the intracellular free copper concentration is kept to an absolute minimum. Several proteins, termed metallochaperones, are charged with the responsibility of delivering copper from membrane transporters to its intracellular destination. The Copper Chaperone for SOD1 (CCS) is the major pathway for SOD1 copper loading. We have determined the first solution structure of hCCS by Small Angle X-ray Scattering (SAXS) in conjunction with size exclusion chromatography (SEC). Our findings highlight the importance of this combined on-line chromatographic technology with SAXS, which has allowed us to unambiguously separate the hCCS dimer from other oligomeric and non-physiological aggregated states that would otherwise adversely effect measurements performed on bulk solutions. Our work exposes the dynamic molecular conformation of this multi-domain chaperone in solution. The metal binding domains known to be responsible for the conveyance of copper to SOD1 can be found in positions that would expedite this movement. Domains I and III of a single hCCS monomer are able to interact and can also move into positions that would facilitate initial copper binding and ultimately transfer to SOD1. Conversely, the interpretation of our solution studies is not compatible with an interaction between these domains and their counterparts in a hCCS dimer. Overall, our results reveal the plasticity of this multi-domain chaperone in solution and are consistent with an indispensable flexibility necessary for executing its dual functions of metal binding and transfer.

Key words: human Cu-chaperone, structural flexibility, multi-domain protein, combined techniques, small-angle X-ray scattering, size exclusion chromatography

To whom correspondence should be addressed (email j.g.grossmann@liv.ac.uk)

INTRODUCTION

The vast majority of species utilise copper as an essential element in aerobic respiration due to its high redox potential [1]. Free soluble copper is a source of oxidative stress because it generates reactive oxygen species through Fenton chemistry [2]. Consequently, the intracellular free copper concentration must be kept to a minimum. It is known to be $\sim 10^{-18}$ M in yeast cells which equates to less than one free copper atom per cell [3]. Under these circumstances it is very unlikely that a newly synthesised copper binding protein will find an amenable copper cofactor without a means of targeting copper to nascent proteins.

Copper uptake and transport into the cell begins with one of the copper transporter family (Ctr) [4]. Copper then passes along an increasing copper affinity gradient that prevents binding by cytoplasmic low molecular weight metal chelators such as metallothioneine and glutathione [5]. Human SOD1 is found in the cytoplasm and the mitochondrial intermembrane space [6, 7]. In each of these locations Copper Chaperone for SOD1 (CCS) interacts directly with SOD1 and can load copper into the newly translated protein [8, 9]. The human CCS homolog was first discovered as a homolog of a yeast protein (Lys7/yCCS), indeed, hCCS is 26% identical to yeast CCS and displays similar domain architecture [8] (Figure 1).

Domain I of both hCCS (residues 1 - 85) and yCCS shows considerable homology to the *S. cerevisiae* Atx1 protein. This region contains a conserved MXCXXC motif seen at the N-terminal region of several copper transport proteins [10, 11] and is known to bind copper (I) [12, 13]. The role of this motif in transfer of copper to SOD1 remains enigmatic however. Substitution of these cysteines results in less than 15% decrease in hCCS activity *in vitro* [14] and one or both may be substituted in a select few species [15]. Furthermore, domain I as a whole is not necessary for yCCS function, except when copper is strictly limited [16]. This may explain the absence of an intact MXCXXC motif in some species. One could hypothesise that copper availability dictates the presence of this functional motif. Domain I is however essential for SOD1 copper loading by hCCS *in vivo* [17].

hCCS domain II (residues 86 - 234) exhibits 50% identity to wild-type hSOD1. Crystallographic studies on the yeast homolog indicated this region harbours the residues involved in formation of both homodimeric yCCS [18] and heterodimeric ySOD1-yCCS [19]. Domain III (residues 235 - 274) is highly conserved among CCS homologs and was proven essential for yCCS function under all conditions indicating this region loads copper into nascent SOD1 [16]. Based on XAS data,

domain III is thought to interact with the MXCXXC motif of domain I and this facilitates copper transfer between these two distal and largely independent regions [20].

While full-length yCCS has been characterised structurally, hCCS is still relatively unknown other than a 2.75 Å resolution crystal structure of the central SOD1-like domain [21] and a solution structure of domain I. Full-length hCCS is described as “difficult” and “recalcitrant” when analysed by crystallisation propensity predictors [22, 23]. The 60 kDa molecular mass of hCCS is beyond the current upper size limit for structural characterisation by solution state NMR.

Small angle X-ray scattering is the method of choice for studying large, flexible biological macromolecules and their complexes in solution. In 2004, *Mathew et al.* [24] documented a combination of the standard SAXS technology with an high performance liquid chromatography (HPLC) apparatus. This synthesis facilitates the separation of impurities, different oligomeric states and aberrant high molecular weight aggregates from the species of interest, by size exclusion chromatography (SEC), directly before exposure to the x-ray beam. It eliminates any averaging contribution from such species and prevents buffer mismatch between blank and sample through the buffer exchange effect of SEC [25]. While this combination of two powerful techniques was demonstrated in 2004, its wider application has not been achieved. The recent installation of a combined SEC-SAXS instrument on the SWING beamline at the French synchrotron SOLEIL [26] has made this technique available to its scientific user community. Here we report the solution structure of human CCS as determined by SEC-SAXS and discuss our findings in the light of the currently received mechanism of copper ion transfer to nascent SOD1.

EXPERIMENTAL

Recombinant hCCS cloning, expression and purification

hCCS coding DNA was amplified by PCR from an IMAGE clone (gi:85567354). PCR products were ligated into the pETM11 expression vector. hCCS expression was performed in BL21 (DE3) *E. coli*. Cultures were grown at 37 °C with agitation until $OD_{600} \sim 0.5$ whereupon expression was induced with 0.4 mM IPTG. Cultures were then incubated at 30 °C overnight with agitation. Harvested cells were resuspended in lysis buffer (20 mM NaH_2PO_4 pH 7.4, 500 mM NaCl, 10 mM imidazole, 5 mM dithiothreitol (DTT), 0.2 mg/ml lysozyme, 10 μ g/ml DNaseI, 1 in 1000 protease inhibitor cocktail set III (Calbiochem)) and lysed by sonication on ice. Insoluble cell debris was separated from the soluble fraction by centrifugation at 30,000 g for 2 hours at 4 °C.

His-tagged hCCS was purified using a His-Trap column (GE Healthcare) then digested with TEV (Tobacco Etch Virus) protease, produced at the University of Liverpool, added to a final concentration of 110 μ g/ml and incubated at 4 °C overnight. Pure protein was dialysed against storage buffer (50 mM Tris-HCl pH 8.0, 150 mM NaCl, 5 mM DTT) and concentrated. Protein was subsequently analysed by SEC on a Superdex 200 16/60 or 10/300 column (GE Healthcare) calibrated with aldolase (158 kDa), bovine serum albumin (BSA, 67 kDa) and ovalbumin (43 kDa) (Sigma).

Small-angle X-ray data collection, processing and interpretation

SAXS data were collected on the SWING beamline at SOLEIL synchrotron, St Aubin, France, using the HPLC integrated SAXS setup [26]. Protein (400 μ g in 40 μ l storage buffer) was loaded onto a pre-equilibrated Shodex KW402.5-4F 150 kDa SEC column at a flow rate of 300 μ l/min at 25 °C before passing through the beam which was set to take 250 frames over the course of protein elution. Scattering was recorded on an AVIEX170x170 CCD detector over an angular range $q_{min} = 0.01 \text{ \AA}^{-1}$ to $q_{max} = 0.5 \text{ \AA}^{-1}$. Data averaging and reduction, including preliminary R_g and $I(0)$ calculations, were carried out using the Foxtrot suite developed at SOLEIL for the SWING beamline. Further analysis was performed with PRIMUS [27], followed by particle distance distribution function $p(r)$ analysis using GNOM [28]. *Ab initio* 3D shape reconstruction was then performed without the imposition of symmetry restraints using the GASBOR web server (EMBL Hamburg) [29]. Thirty models were averaged with DAMAVER [30] and the resulting structures compared with the crystal structure of domain II hCCS in PyMOL [31].

The published crystal structure of hCCS domain II [21] was used as a the structural model for the hCCS amino acid region 88 - 232. The secondary structure of region 12 – 69 was inferred using models of the Atx1-like domain I proposed by the I-TASSER web server [32]. Similarly, the secondary structure of the short α -helix found in domain III, amino acids 250 – 258, was inferred using I-TASSER. Terminal and linker regions 1 – 11 (with the addition of two extra amino acids remaining from TEV cleavage of the hexa-histidine tag), 70 – 87, 233 – 249 and 259 – 274 are predicted to be unstructured. The rigid body modelling software BUNCH [33] was then used to generate 25 hCCS models constrained by the position of the SOD1-like domain II that forms the interface between two CCS monomers. Unrestrained movement of domain I and III together with the flexible linker regions was permitted. BUNCH only generates C α -atom positions for flexible structural segments such as linkers and peptide terminal ends. The protein backbone and sidechain positions of these flexible regions were reconstructed from their C α traces using the SABBAC web server [34]. The scattering profile of each reconstructed and complete model was then computed with CRY SOL [35].

RESULTS & DISCUSSION

Characterisation of recombinant hCCS and static SAXS measurements

hCCS produced as described has a molecular mass of 29.2 kDa and contains a stoichiometric amount of zinc but negligible copper as determined by electrospray ionisation MS and inductively coupled ionisation MS respectively. When examined by SEC a dominant peak at ~60 kDa is observed indicating that hCCS is predominantly dimeric. Tetrameric protein that elutes prior to the dimeric form is observed as previously described by *Winkler et al.* [36]. Aggregated protein that elutes from the column in the void volume is also observed (Figure 2A). When dimeric protein is separated and stored, these higher molecular weight species reform and eventually lead to extensive aggregation of the protein (Figure 2A inset). Standard SAXS experiments on recombinant hCCS at synchrotron beamlines at both SSRL (BL4-2, Stanford, USA [37]) and SPring-8 (BL45XU, Harima, Japan [38]) yielded incongruence in scattering profiles and deduced structural parameters (Table 1, Figure 3A), such as substantially increased values for the radius of gyration (R_g), indicating a problem with protein monodispersity.

Measurement of hCCS in solution by combined SEC-SAXS

In order to overcome oligomerisation in bulk solutions it was crucial to isolate dimeric hCCS immediately prior to X-ray analysis. Scattering experiments were therefore performed on the SWING beamline at SOLEIL using the SEC-SAXS set-up [26]. This system combines an optimised synchrotron radiation SAXS instrument with high performance liquid chromatography sample delivery. Human CCS samples at a concentration of 10 mg/ml were passed along a Shodex KW402.5-4F 150 kDa SEC column before exposure to the X-ray beam.

Scattering data were collected over the course of protein elution with approximately 20 frames taken before protein reached the beam for background subtraction purposes. Figure 2B shows information extracted over the course of the SAXS measurements for hCCS with approximate R_g and $I(0)$ values indicating the heterogeneity of the sample. The $I(0)$ value is directly related to protein concentration and reflects the SEC UV absorption profile. The region with highest protein concentration and steady R_g values was identified and averaged. Prior to this peak significantly higher R_g values were observed pointing to the presence of larger molecular weight species. Subsequent examination yields a R_g value of 31.3 ± 0.81 Å and a maximum particle dimension (D_{\max}) of 118 ± 5 Å (Table 1, Figure 3 inset) supporting the notion that the hCCS dimer is

significantly larger than the crystal structure of the equivalent dimer from yeast [18] that yields $R_g = 25.9 \text{ \AA}$ and $D_{\max} = 85 \text{ \AA}$. Each monomer in this structure has a predicted molecular mass of 25.8 kDa as opposed to the 29.1 kDa recombinant hCCS used in this study. This molecular mass difference is a contributor to the R_g and D_{\max} value disparity.

Quaternary structure of hCCS and a mechanism of copper transfer to SOD1

Low-resolution 3D models of the hCCS dimer were restored using the *ab initio* shape reconstruction program GASBOR [29]. These models were used to examine the overall shape and possible domain arrangements of hCCS (Supplementary Figure S1). Given the flexible nature of full-length hCCS, however, it is not expected to exist as a static, globular macromolecule in solution. hCCS is more likely to exhibit conformational plasticity with domains I and III able to move freely with respect to domain II. In order to explore the conformational space occupied by hCCS and the biologically relevant interactions between these domains we modelled their arrangement and positions using the program BUNCH [33] in conjunction with models of the three hCCS domains (Figure 1A, B and C). This provides a more plausible dynamic structural depiction of the hCCS dimer in solution (Figure 4A).

Each different rigid body model generated by this process is consistent with the SAXS data as indicated by a very good scattering profile fit to the experimental results (Figure 3B). These models collectively, therefore, represent a pool of potential domain arrangements hCCS could adopt in solution. Figure 4B indicates domain I forms a hemispherical halo around the central SOD1-like domain II and appears to be constrained by the length of the interdomain linker. In contrast however, domain III does not appear to be constrained as such and forms an extension into the solvent that is free to move. These models highlight the possibility of an interaction between the Cu(I) binding regions of domains I and III from each monomer as described by *Eisses et al.* [20]. Conversely, there is no obvious indication of a domain swap between the two hCCS monomers. The possibility of a domain I-I or domain III-III interaction is also unlikely due to their spatial separation. Figure 4B illustrates how the various hCCS conformations, directly observed here for the first time, fit into the presently accepted mechanism of copper transfer from membrane bound copper transporter Ctr1 through hCCS and the eventual delivery to SOD1 via an increasing Cu(I) affinity gradient [5].

Domain I is essential for hCCS mediated incorporation of copper into SOD1 [17]. Reversible copper transfer has been observed between Ctr1 and Atx1 [39] and is likely to proceed in a similar

fashion between Ctr1 and hCCS domain I. The initial stage of copper binding by domain I is illustrated by the model represented in Figure 4Bi where domain I is found to be free, solvent exposed and receptive. This would permit copper transfer to the Atx1-like domain from the C-terminus of hCtr1 while hCCS is in the dimer state. As with the succeeding steps in this process, initial acquisition seems to occur independently for each hCCS monomer due to the lack of interaction between opposing domains.

C-terminal domain III is then able to acquire copper from domain I. This is facilitated by a conformation in which the two domains are physically adjacent (Figure 4Bii). Sufficient space is present in this model for the adoption of a large multi-nuclear copper-sulphur cluster between the copper binding cysteines of each domain. In the absence of SOD1, this cluster formation presents a favourable and secure retention pocket for Cu(I) ions which may lead to a conformational change [40] that facilitates hCCS homodimer dissociation enabling realisation of the SOD1-CCS heterodimer.

Ultimately copper loaded domain III is then able to move toward the empty copper site of SOD1 (in Figure 4Biii this is represented by replacement of the SOD1-like domain of the opposing hCCS monomer with a wild-type SOD1 monomer, PDB code 2VOA [41]). It is important to note that these models represent hCCS in solution and were generated directly from scattering data without the need to artificially constrain model building in order to demonstrate domain interactions as has previously been documented using *in silico* methods [42].

While the models presented here lend themselves to a demonstration of the feasibility of copper movement between domains they do not represent the complete spectrum of possible hCCS conformations. It is possible a mixture of conformations exist that satisfy the experimental data in totality but individually do not. Thus hyper-extended and compact structures may coexist in solution. Currently there is no substantiated and non-circuitous means to determine the composition of such a conformationally heterogeneous solution for oligomeric proteins. This limitation does not detract however from the message foregrounded here.

The main pathway for SOD1 activation is by its cognate chaperone; CCS [8, 9]. The hCCS models delineated by the X-ray solution scattering analysis indicate hCCS exists in a range of conformations with highly independent domains. The models propose a system whereby domains I and III of one hCCS monomer are able to interact with each other but not with their dimer counterparts.

The size and flexibility of hCCS has thus far prohibited its structural characterisation. The analysis described here is the first structural characterisation of full-length human CCS in solution and would not have been possible without the combination of two complementary methods. It highlights the efficacy of the SAXS-HPLC technique for the analysis of biological macromolecules that exhibit variable oligomeric states or a propensity to aggregation. Having measured recombinant hCCS at several SAXS beamlines we find those observations obtained by the use of this combined technique to remove many of the pitfalls associated with static SAXS experiments.

ACKNOWLEDGEMENTS

We thank the following synchrotron radiation facilities for beamtime on their SAXS instruments: SOLEIL (SWING), France; SSRL (BL4.2), USA and SPring-8 (BL45XU), Japan. In particular we are very much indebted to Dr. Javier Pérez (SOLEIL), Dr. Hirotsugu Tsuruta (SSRL) and Dr. Takaaki Hikima (SPring-8) for their help with SAXS data acquisition. Access to SOLEIL was provided via a trans-national access program. We are grateful to the University of Liverpool and the Motor Neuron Disease Association (grant reference : Hasnain/Mar09/6055) for their support.

The molecular coordinate files generated during the course of this work are available upon request to the authors.

Accepted Manuscript

TABLES

Table 1. Structural parameters with errors derived from SAXS experiments of hCCS collected at three different synchrotron radiation facilities.

SR Facility	SPring-8	SSRL	SOLEIL
Beamline	BL45XU [38]	BL4-2 [37]	SWING [26]
R_g (Å)	60.1±0.3	38.3±0.3	31.4±0.1
D_{max} (Å)	189±8	160±7	118±5

Position within the text: following paragraph 1 of Results and Discussion.

Accepted Manuscript

FIGURES & CAPTIONS

Figure 1. Multiple sequence alignment of hCCS with similar proteins and structural representations of the three hCCS domains generated by homology modelling.

The three hCCS domains are highlighted in the sequence alignment with (A) the predicted structure of the Atx-1 like domain I (37% identity with *S. cerevisiae* Atx1), (B) the crystal structure of SOD1-like domain II monomer (50% identity with hSOD1) and (C) the predicted structure of domain III. Copper binding regions are also indicated in red.

Figure 2. Size exclusion chromatography and SAXS measurements of recombinant hCCS.

(A) 17 mg of hCCS was loaded onto a calibrated Superdex 200 16/60 gel filtration column in a 1 ml volume. Inset, aggregated hCCS after extended incubation at 4°C on Superdex 200 10/300 column. (B) hCCS R_g and $I(0)$ acquired on the SEC-SAXS setup at SWING. Values were determined from scattering data, plotted over a time course of elution of hCCS from the SEC column represented here as frame number of exposure to the X-ray beam. Frames 168 – 175 used for subsequent analysis are highlighted gray.

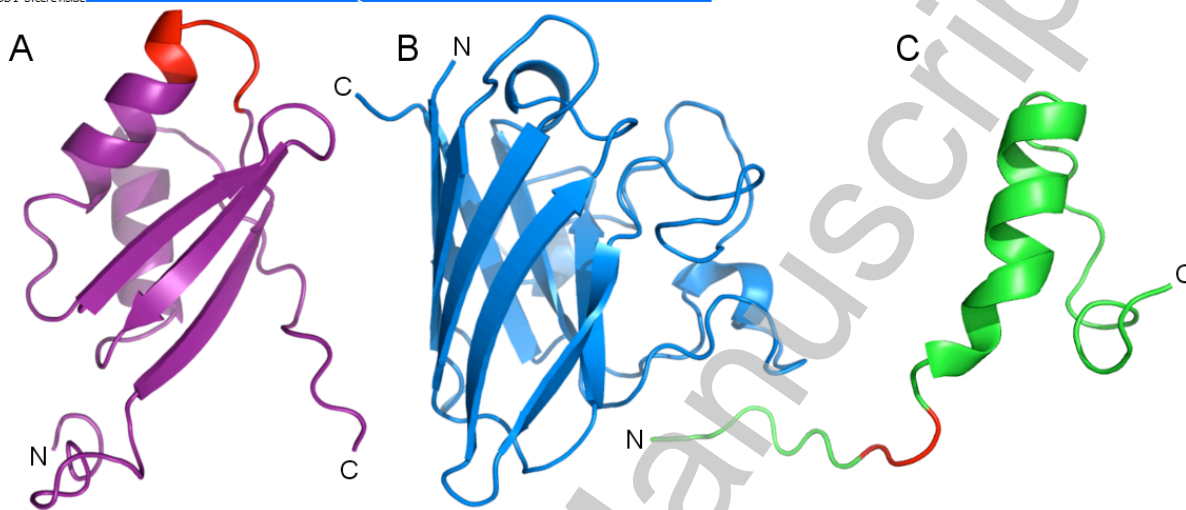
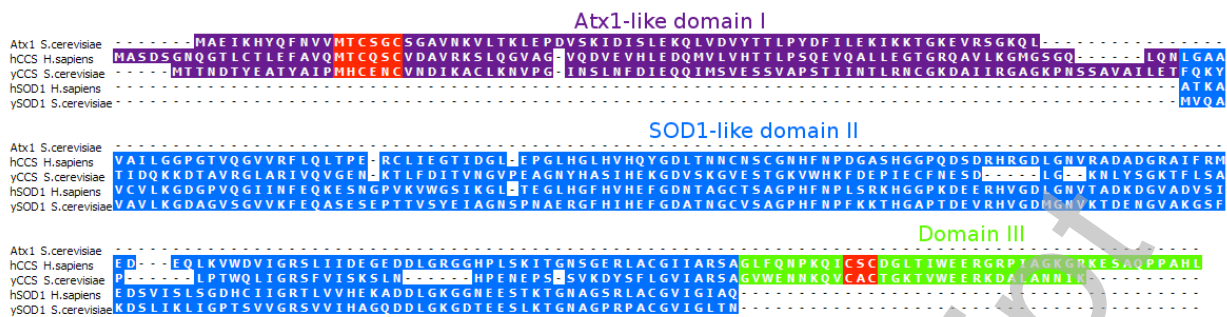
Figure 3. SAXS data analysis.

(A) Low-angle regions of X-ray scattering data collected for recombinant hCCS shown in the form of Guinier plots. The Guinier region is defined by $q < 1.3/R_g$ (highlighted with grey symbols). Scattering data were acquired at SPring-8 (\square), SSRL (\circ) and SWING, SOLEIL (Δ) with the combined HPLC-SAXS equipment (see Table 1 for a comparison of experimentally derived structural parameters). The upper plot generated from data acquired at SPring-8 clearly indicates the presence of aggregated sample. (B) The experimental scattering profile (with error bars) of recombinant hCCS from the combined SEC/SAXS study. The SAXS curve resulted from the small number of frames as indicated in Figure 2B. Black curves represent fits from individual rigid body models (see Figure 4) against the experimental scattering profile of hCCS. The goodness-of-fit value (χ^2) varies between 1.7 and 2.1. Inset, the deduced distance distribution function $p(r)$ with error bars (10^1)

Figure 4. The structural plasticity of hCCS deduced from SAXS

(A) Twenty-five hCCS structures derived by rigid body modelling against experimental SAXS data rotated 180° around the long axis with the crystal structure of yCCS in the same orientation given for comparison. Domains are coloured according to Figure 1, I-purple, II-blue, III-green, copper binding motifs are depicted in red, yCCS is pink. (B) The mechanism of hCCS mediated copper delivery to SOD1 illustrated using the models generated above: three hCCS models, with flexible linker regions reconstructed from their $C\alpha$ positions, representing the stages of copper transfer in one monomer. (i) The MXCXXC motif of domain I is exposed, facilitating copper transfer from the membrane bound copper transport protein Ctr1, as is the CXC motif of domain III, $\chi^2 = 1.7$. (ii) The copper binding motifs of domains I and III are able to interact allowing copper sequestration and subsequent transfer, $\chi^2 = 2.0$. (iii) Domain III is able to move toward domain II of the opposing hCCS monomer here represented by a SOD1 monomer (gold), $\chi^2 = 2.0$.

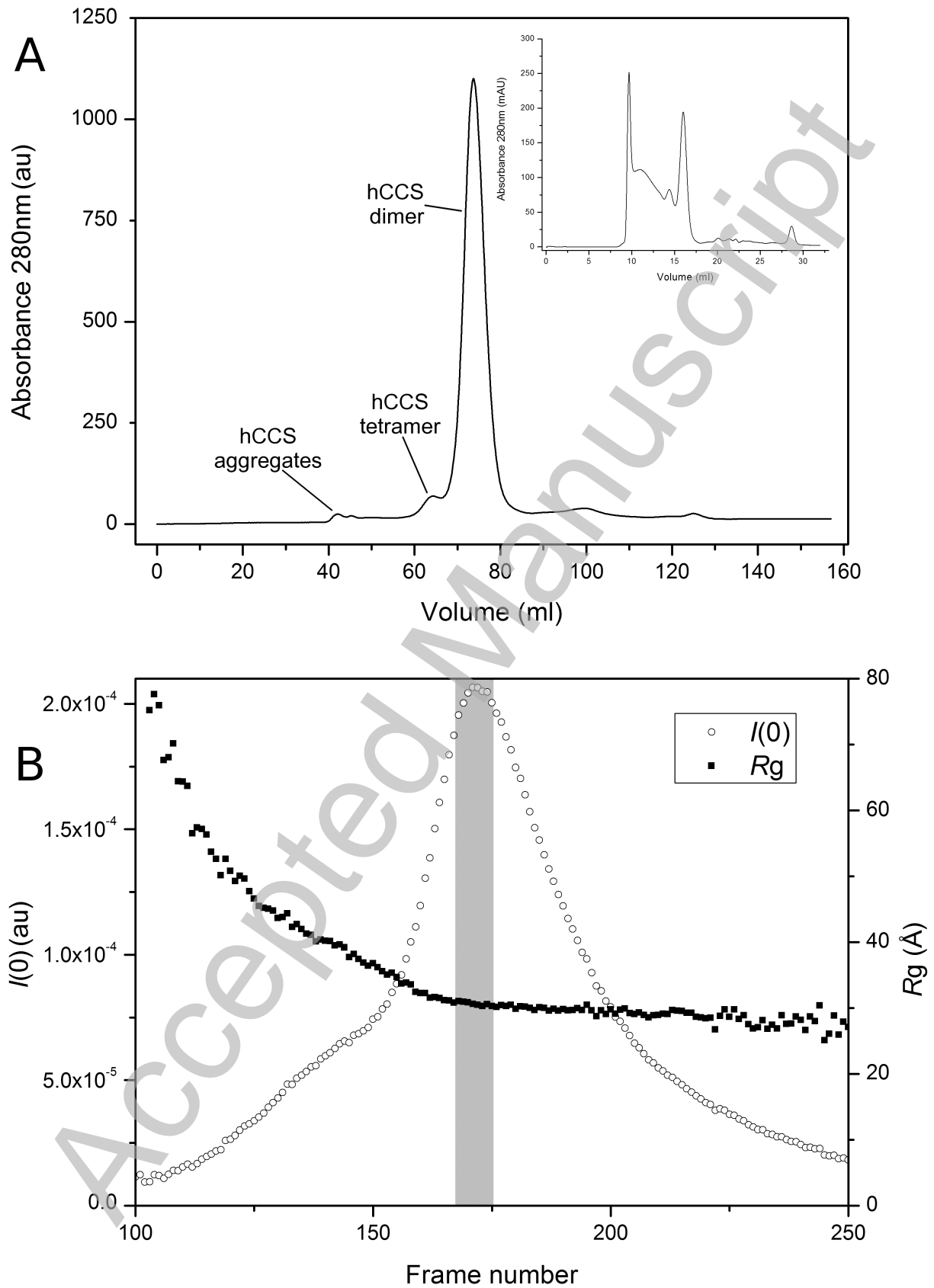
Figure 1



THIS IS NOT THE VERSION OF RECORD - see doi:10.1042/BJ20110948

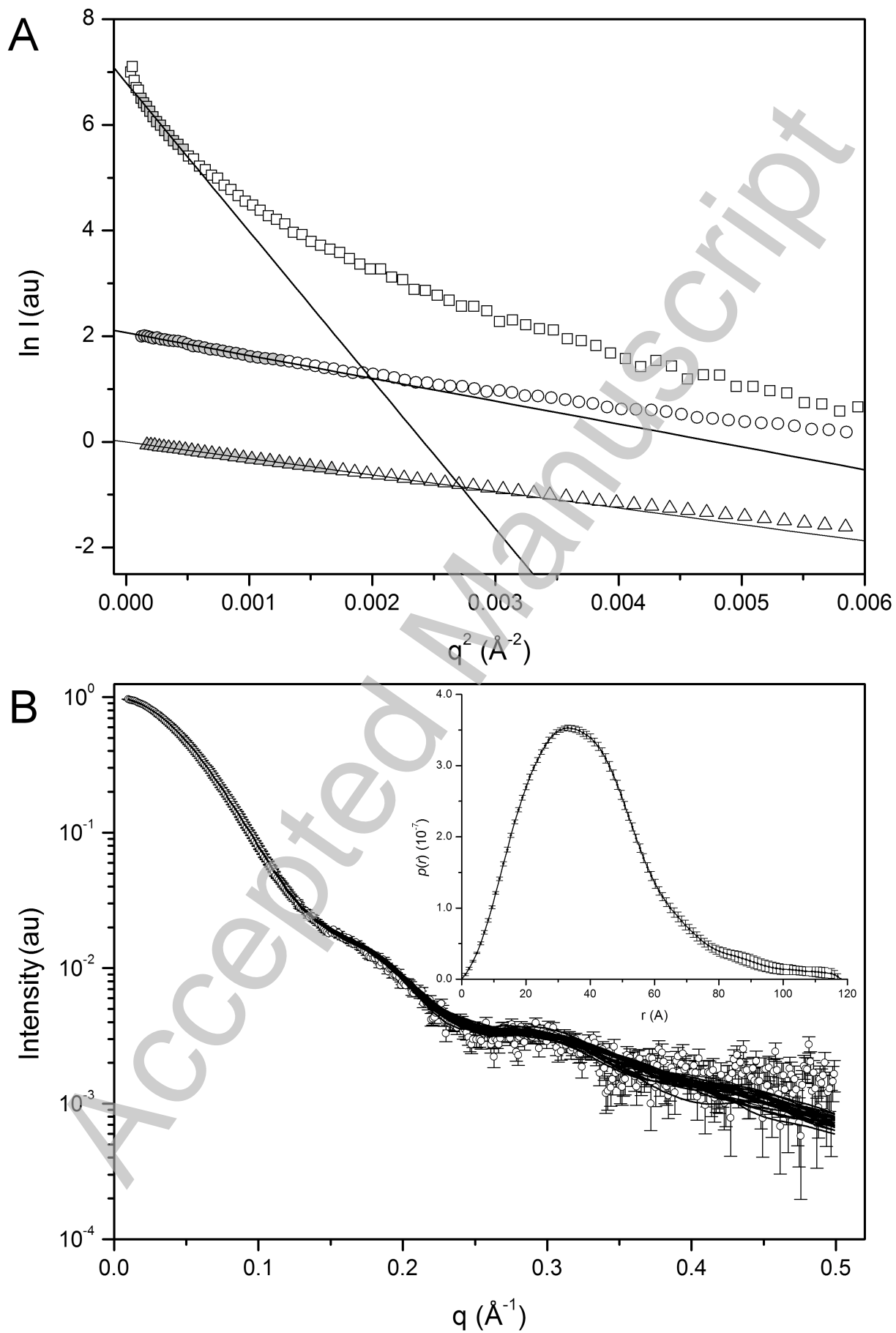
Accepted Manuscript

Figure 2



THIS IS NOT THE VERSION OF RECORD - see doi:10.1042/BJ20110948

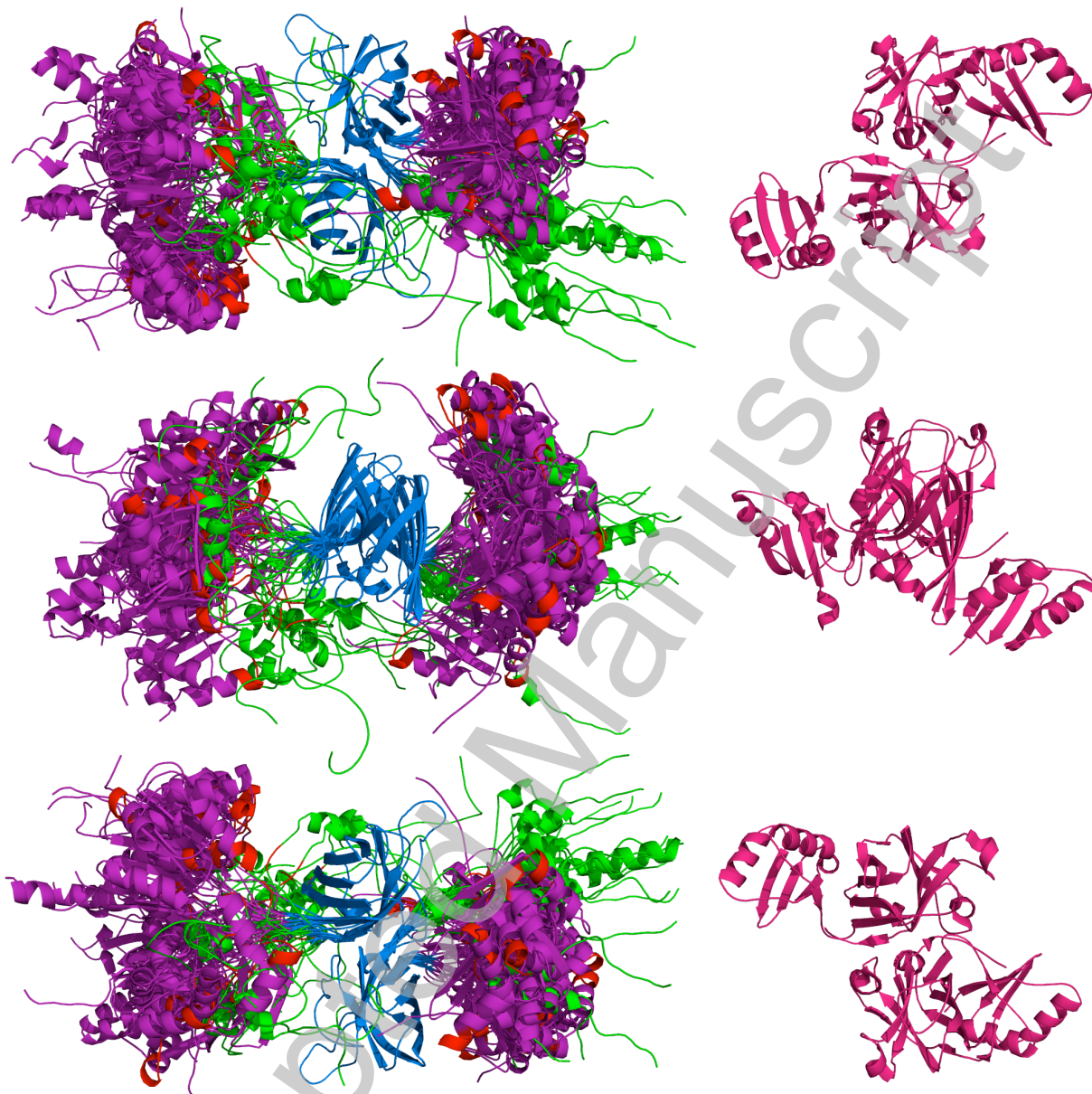
Figure 3



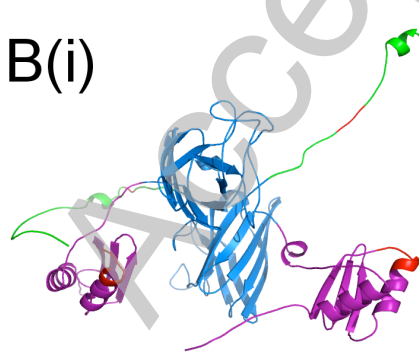
THIS IS NOT THE VERSION OF RECORD - see doi:10.1042/BJ20110948

Figure 4

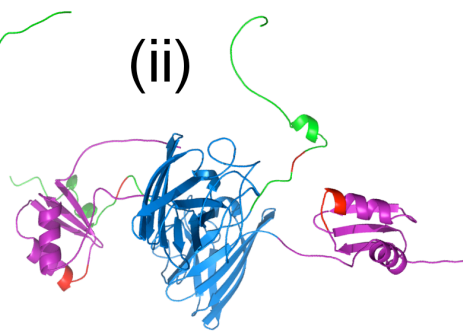
A



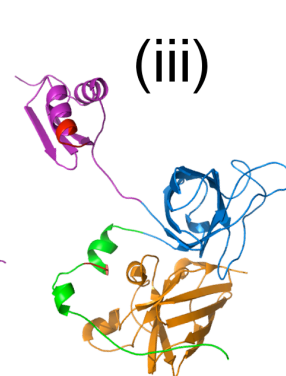
B(i)



(ii)



(iii)



REFERENCES

1. Andreini, C., Banci, L., Bertini, I. and Rosato, A. (2008) Occurrence of copper proteins through the three domains of life: a bioinformatic approach. *J. Proteome Res.* **7**, 209-216.
2. Gaetke, L. M., and Chow, C. K. (2003) Copper toxicity, oxidative stress, and antioxidant nutrients. *Toxicology* **189**, 147-163.
3. Rae, T. D., Schmidt, P. J., Pufahl, R. A., Culotta, V. C. and O'Halloran, T. V. (1999) Undetectable intracellular free copper: the requirement of a copper chaperone for superoxide dismutase. *Science* **284**, 805-808.
4. Zhou, B. and Gitschier, J. (1997) hCTR1: a human gene for copper uptake identified by complementation in yeast. *Proc. Natl. Acad. Sci. U.S.A* **94**, 7481-7486.
5. Banci, L., Bertini, I., Ciofi-Baffoni, S., Kozyreva, T., Zovo, K. and Palumaa, P. (2010) Affinity gradients drive copper to cellular destinations. *Nature* **465**, 645-648.
6. Crapo, J. D., Oury, T., Rabouille, C., Slot, J. W. and Chang, L. Y. (1992) Copper,zinc superoxide dismutase is primarily a cytosolic protein in human cells. *Proc. Natl. Acad. Sci. U.S.A* **89**, 10405-10409.
7. Okado-Matsumoto, A. and Fridovich, I. (2001) Subcellular distribution of superoxide dismutases (SOD) in rat liver: Cu,Zn-SOD in mitochondria. *J. Biol. Chem.* **276**, 38388-38393.
8. Culotta, V. C., Klomp, L. W., Strain, J., Casareno, R. L., Krems, B. and Gitlin, J. D. (1997) The copper chaperone for superoxide dismutase. *J. Biol. Chem.* **272**, 23469-23472.
9. Casareno, R. L., Waggoner, D. and Gitlin, J. D. (1998) The copper chaperone CCS directly interacts with copper/zinc superoxide dismutase. *J. Biol. Chem.* **273**, 23625-23628.
10. Yamaguchi, Y., Heiny, M. E. and Gitlin, J. D. (1993) Isolation and characterization of a human liver cDNA as a candidate gene for Wilson disease. *Biochem. Biophys. Res. Commun.* **197**, 271-277.
11. Chelly, J., Tümer, Z., Tønnesen, T., Petterson, A., Ishikawa-Brush, Y., Tommerup, N., Horn, N. and Monaco, A. P. (1993) Isolation of a candidate gene for Menkes disease that encodes a potential heavy metal binding protein. *Nat. Genet.* **3**, 14-19.
12. Anastassopoulou, I., Banci, L., Bertini, I., Cantini, F., Katsari, E. and Rosato, A. (2004) Solution structure of the apo and copper(I)-loaded human metallochaperone HAH1. *Biochemistry* **43**, 13046-13053.
13. Arnesano, F., Banci, L., Bertini, I., Huffman, D. L. and O'Halloran, T. V. (2001) Solution structure of the Cu(I) and apo forms of the yeast metallochaperone, Atx1. *Biochemistry* **40**, 1528-1539.
14. Stasser, J. P., Siluvai, G. S., Barry, A. N. and Blackburn, N. J. (2007) A multinuclear copper(I) cluster forms the dimerization interface in copper-loaded human copper chaperone for superoxide dismutase. *Biochemistry* **46**, 11845-11856.
15. Kirby, K., Jensen, L. T., Binnington, J., Hilliker, A. J., Ulloa, J., Culotta, V. C. and Phillips, J. P. (2008) Instability of superoxide dismutase 1 of *Drosophila* in mutants deficient for its cognate copper chaperone. *J. Biol. Chem.* **283**, 35393-35401.
16. Schmidt, P. J., Rae, T. D., Pufahl, R. A., Hamma, T., Strain, J., O'Halloran, T. V. and Culotta, V. C. (1999) Multiple protein domains contribute to the action of the copper chaperone for superoxide dismutase. *J. Biol. Chem.* **274**, 23719-23725.
17. Caruano-Yzermans, A. L., Bartnikas, T. B. and Gitlin, J. D. (2006) Mechanisms of the copper-dependent turnover of the copper chaperone for superoxide dismutase. *J. Biol. Chem.* **281**, 13581-13587.
18. Lamb, A. L., Wernimont, A. K., Pufahl, R. A., Culotta, V. C., O'Halloran, T. V. and Rosenzweig, A. C. (1999) Crystal structure of the copper chaperone for superoxide dismutase. *Nat. Struct. Biol.* **6**, 724-729.
19. Lamb, A. L., Torres, A. S., O'Halloran, T. V. and Rosenzweig, A. C. (2001) Heterodimeric structure of superoxide dismutase in complex with its metallochaperone. *Nat. Struct. Biol.* **8**, 751-755.

20. Eisses, J. F., Stasser, J. P., Ralle, M., Kaplan, J. H. and Blackburn, N. J. (2000) Domains I and III of the human copper chaperone for superoxide dismutase interact via a cysteine-bridged Dicopper(I) cluster. *Biochemistry* **39**, 7337-7342.
21. Lamb, A. L., Wernimont, A. K., Pufahl, R. A., O'Halloran, T. V. and Rosenzweig, A. C. (2000) Crystal structure of the second domain of the human copper chaperone for superoxide dismutase. *Biochemistry* **39**, 1589-95.
22. Overton, I. M., Padovani, G., Girolami, M. A. and Barton, G. J. (2008) ParCrys: a Parzen window density estimation approach to protein crystallization propensity prediction. *Bioinformatics* **24**, 901-907.
23. Slabinski, L., Jaroszewski, L., Rychlewski, L., Wilson, I. A., Lesley, S. A. and Godzik, A. (2007) XtalPred: a web server for prediction of protein crystallizability. *Bioinformatics* **23**, 3403-3405.
24. Mathew, E., Mirza, A. and Menhart, N. (2004) Liquid-chromatography-coupled SAXS for accurate sizing of aggregating proteins. *J. Synchrotron Rad.* **11**, 314-318.
25. Porath, J. and Flodin, P. (1959) Gel Filtration: A method for desalting and group separation. *Nature* **183**, 1657-1659.
26. David, G. and Perez, J. (2009) Combined sampler robot and high-performance liquid chromatography: a fully automated system for biological small-angle X-ray scattering experiments at the Synchrotron SOLEIL SWING beamline. *J. Appl. Cryst.* **42**, 892-900.
27. Konarev, P. V., Volkov, V. V., Sokolova, A. V., Koch, M. H. J. and Svergun, D. I. (2003) PRIMUS: a Windows PC-based system for small-angle scattering data analysis. *J. Appl. Cryst.* **36**, 1277-1282.
28. Svergun, D. I. (1992) Determination of the regularization parameter in indirect-transform methods using perceptual criteria. *J. Appl. Cryst.* **25**, 495-503.
29. Svergun, D. I., Petoukhov, M. V. and Koch, M. H. (2001) Determination of domain structure of proteins from X-ray solution scattering. *Biophys. J.* **80**, 2946-2953.
30. Volkov, V. and Svergun, D. (2003) Uniqueness of ab initio shape determination in small-angle scattering. *J. Appl. Cryst.* **36**, 860-864.
31. The PyMOL Molecular Graphics System. Schrödinger, LLC.
32. Roy, A., Kucukural, A. and Zhang, Y. (2010) I-TASSER: a unified platform for automated protein structure and function prediction. *Nat. Protoc.* **5**, 725-738.
33. Petoukhov, M. V. and Svergun, D. I. (2005) Global Rigid Body Modeling of Macromolecular Complexes against Small-Angle Scattering Data. *Biophys. J.* **89**, 1237-1250.
34. Maupetit, J., Gautier, R. and Tufféry, P. (2006) SABBAC: online Structural Alphabet-based protein Backbone reconstruction from Alpha-Carbon trace. *Nucleic Acids Res.* **34**, W147-151.
35. Svergun, D., Barberato, C. and Koch, M. CRY SOL - a Program to Evaluate X-ray Solution Scattering of Biological Macromolecules from Atomic Coordinates. *J. Appl. Cryst.* **28**, 768-773.
36. Winkler, D. D., Schuermann, J. P., Cao, X., Holloway, S. P., Borchelt, D. R., Carroll, M. C., Proescher, J. B., Culotta, V. C. and Hart, P. J. (2009) Structural and biophysical properties of the pathogenic SOD1 variant H46R/H48Q. *Biochemistry* **48**, 3436-3447.
37. Smolsky, I. L., Liu, P., Niebuhr, M., Ito, K., Weiss, T. M. and Tsuruta, H. (2007) Biological small-angle X-ray scattering facility at the Stanford Synchrotron Radiation Laboratory. *J. Appl. Cryst.* **40**, s453-s458.
38. Fujisawa, T., Inoue, K., Oka, T., Iwamoto, H., Uruga, T., Kumasaka, T., Inoko, Y., Yagi, N., Yamamoto, M. and Ueki, T. (2000) Small-angle x-ray scattering station at the SPring-8 RIKEN beamline. *J. Appl. Cryst.* **33**, 797-800.
39. Xiao, Z. and Wedd, A. G. (2002) A C-terminal domain of the membrane copper pump Ctr1 exchanges copper(I) with the copper chaperone Atx1. *Chem. Commun. (Camb.)* 588-589.
40. Rae, T. D., Torres, A. S., Pufahl, R. A. and O'Halloran, T. V. (2001) Mechanism of Cu,Zn-superoxide dismutase activation by the human metallochaperone hCCS. *J. Biol. Chem.* **276**, 5166-5176.

41. Strange, R. W., Yong, C. W. Smith, W. and Hasnain, S. S. (2007) Molecular dynamics using atomic-resolution structure reveal structural fluctuations that may lead to polymerization of human Cu-Zn superoxide dismutase. *Proc. Natl. Acad. Sci. U.S.A* **104**, 10040-10044.
42. Falconi, M., Iovino, M. and Desideri, A. (1999) A model for the incorporation of metal from the copper chaperone CCS into Cu,Zn superoxide dismutase. *Structure* **7**, 903-908.

Accepted Manuscript

THIS IS NOT THE VERSION OF RECORD - see doi:10.1042/BJ20110948